Journal of Manufacturing Processes 58 (2020) 510–523

Contents lists available at ScienceDirect

Journal of Manufacturing Processes

journal homepage: www.elsevier.com/locate/manpro

Technical Paper

Tool path design system to enhance accuracy during double sided incremental forming: An analytical model to predict compensations for small/large components

K. Praveen, R. Lingam, N. Venkata Reddy*

Department of Mechanical and Aerospace Engineering, Indian Institute of Technology Hyderabad, Kandi 502285, Telangana, India

ARTICLE INFO

Keywords:
Double sided incremental forming
Membrane theory
Compensated tool path generation
Accuracy

ABSTRACT

Double sided incremental forming (DSIF) has potential to form complex three-dimensional sheet metal components without using component specific tooling. Forming tool deflection and sheet spring-back are significant factors contributing to the geometrical inaccuracy of DSIF components. Numerical prediction and experimental measurement of sheet spring-back is time consuming. In addition, available analytical methods to predict and compensate sheet spring-back uses theory of small deflections by neglecting the membrane effects. With increase in sheet deflection beyond its thickness, membrane forces experienced by the middle plane of sheet due to stretching significantly resists the applied transverse load. In the present work, combination of small deflection and membrane theories are used to predict and compensate sheet deflections, so that a single methodology can be used for small as well as large components. Proposed methodology is validated using experimental and numerical predictions and they are in very good agreement. Two geometries (axisymmetric, free form components) with different component openings are formed to validate the proposed predictive methodology. Results indicate there is significant improvement (maximum error is less than 800 μm) in accuracy of components formed using compensated tool paths developed using proposed model. In addition, support tool maintained contact with component throughout forming (maximum force on the support tool is less than 60 N).

1. Introduction

Incremental sheet forming (ISF) is a die-less forming process that uses hemispherical/spherical or other shaped ended tools to form the sheet progressively by a series of local deformations. Capabilities and challenges of ISF process have been summarized by various researchers [1–12]. Double sided incremental forming (DSIF) process is the most flexible variant of ISF processes. DSIF uses two tools, at any instant one tool will be forming the geometry while other provides local support [2,9,13]. Two tools can swap their roles depending on the geometric characteristics of the shape being formed. This process not only gives the flexibility to form features on both sides of sheet but also reduces/eliminates the unwanted bending at component opening. However, continuous spring-back of sheet during forming and also forming tool deflection (Fig. 1) will result in less accurate component [1,5,10,14]. Various researchers have tried to improve the accuracy of ISF components either by applying compensations for errors or using different forming strategies. Compensation methodologies are based on experimental measurements [14–18], analytical predictions [19–23] and regression model obtained using numerically predicted force–deflection data [24]. Forming strategies include local heating in deformation zone [25,26], squeezing tool path in DSIF [13,27–29], in-to-out tool path in Accumulated DSIF [30,31].

Ambrogio et al. [14] studied the effect of tool diameter and incremental depth on geometrical accuracy in single point incremental forming (SPIF) of a truncated pyramid component having opening size of 163 mm. They showed that elastic spring-back of sheet and bending at component opening (in the absence of backing plate) are the major causes for geometrical inaccuracies. Hirt et al. [15] proposed an experimental method to improve geometrical accuracy of SPIF components. They formed a truncated pyramid of 180 mm opening size and measured its geometry using coordinate measuring machine. The deviations at measured locations to that of corresponding target geometry are used to correct the tool path. They reported that the maximum deviation of measured profile to that of ideal profile is reduced from 2.5 mm to 1.5 mm by using corrected tool path. Ambrogio et al. [16] studied the effect of process (incremental depth, tool diameter) and geometrical parameters (wall angle, depth of component, thickness of

* Corresponding author.
E-mail address: nvr@iith.ac.in (N. Venkata Reddy).

https://doi.org/10.1016/j.jmapro.2020.08.014
Received 31 December 2019; Received in revised form 13 June 2020; Accepted 5 August 2020
Available online 28 August 2020

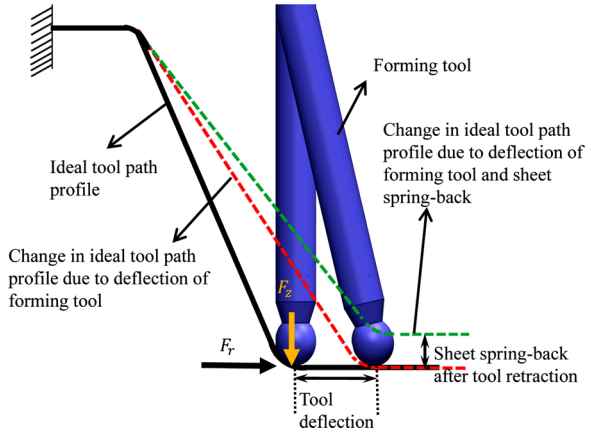

Fig. 1. Schematic showing the forming tool deflection due to radial force (F_r) and sheet spring-back after tool retraction (F_z: axial force).

sheet material) on the profile deviation of a truncated pyramid component having opening size of 100 mm. A regression model is developed by them to obtain the errors as a function of process and geometric parameters. Behera et al. [17] proposed a tool path compensation strategy to improve geometrical accuracy of SPIF components using multivariate adaptive regression splines (MARS) model. The MARS model was trained using the error between measured and ideal CAD geometry for several patch interactions (planar, ribs, free-form). Trained MARS engine is used to sequence the patches and adjust the CAD model which is used for tool path generation. Maximum deviation of the pyramid component (opening size of 150 mm) formed using compensated tool path was 1 mm. Allwood et al. [18] demonstrated a closed loop control strategy using spatial impulse responses to enhance the accuracy in SPIF with feedback provided by a stereo-vision camera. Weibull distribution curve was developed to predict the spatial impulses using the error between measured and ideal profiles. For a conical geometry having component opening of 120 mm formed using closed loop control strategy and reduced the absolute error from 2.5 mm to 0.2 mm. Asghar et al. [19] developed a mechanics based methodology to predict and compensate sheet and tool deflections in SPIF and validated it for different geometries namely truncated cone, varying wall angle cone and free-form geometry. For a conical component of 60° wall angle and component opening of 70 mm, maximum profile deviation is reduced from 1.2 mm to 0.3 mm by using compensated tool path. For a varying wall angle component, maximum profile deviation reduced from 1.5 mm to 0.6 mm by using compensated tool path. However, their sheet deflection prediction methodology is valid only when deflections are small compared to sheet thickness. Duflou et al. [25,26] used local heating in deformation zone to reduce forming forces and spring-back to enhance accuracy of SPIF components. They reported that maximum profile deviation in the case of a conical component of 40° wall angle (opening size of 160 mm) is reduced from 3.5 mm to 1.5 mm by using local heating strategy.

In SPIF process, bending of sheet between fixture and component opening takes place due to absence of support. To avoid bending at component opening, Yoshikawa et al. [32] used two tools for performing incremental forming. A large flat ended tool is moved along the component opening to provide support and small spherical tool is used to form the geometry. Reddy et al. [33] used two tools moving in synchronized manner to form components having features on either side of sheet. At any instant one tool will be forming the geometry while other provides local support. Meier et al. [13] used two robot arms to perform DSIF process. They used position control for forming tool and position as well as force control for support tool to ensure continuous contact. Vision-based 3D surface scanner was employed to estimate

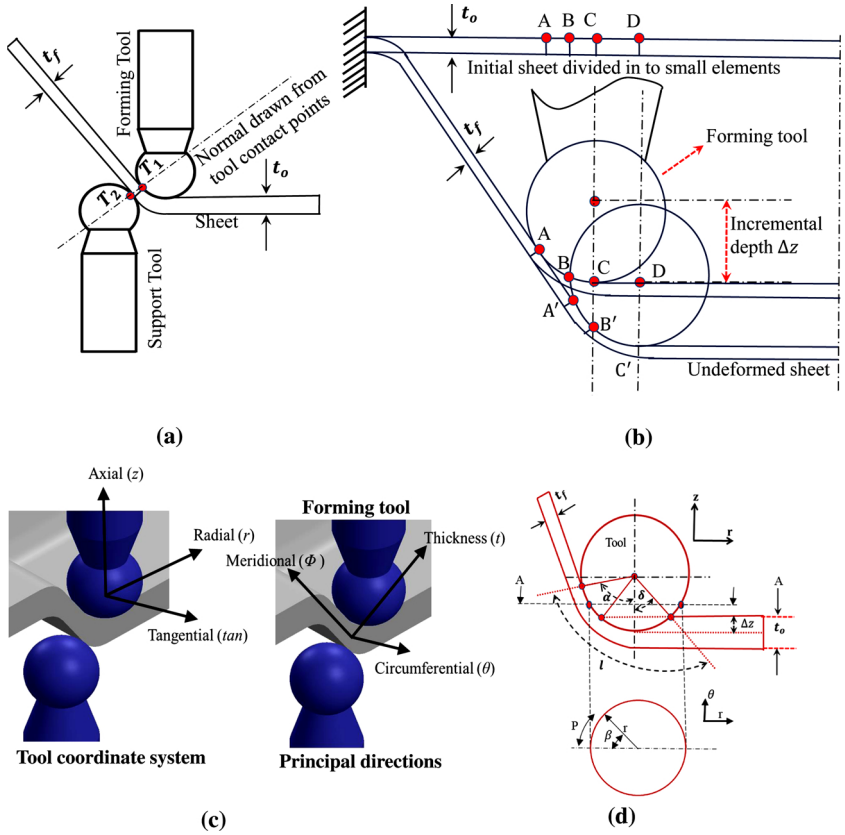

Fig. 2. (a) Tool configuration, (b) schematic showing the material movement to predict deformed sheet thickness [39], (c) tool coordinate system and principal directions, and (d) schematic showing the tool-sheet contact area calculation [40].

deviations from the ideal profile and to modify tool path to enhance the accuracy. Profile deviation in the wall region of a truncated cone of opening 90 mm and depth of 40 mm has reduced from 1.5 mm to 0.25 mm by using modified tool path. However, deviation of 0.5 mm to 1.0 mm is reported in the regions near the component opening as well as at the base region. Malhotra et al. [27] carried out an experimental investigation on DSIF of a 65° cone (opening size of 132 mm) using squeezed tool path. Squeeze factor is defined as the ratio of the distance between tool contact points (Fig. 2(a)) to that of thickness predicted using sine law. They reported that the support tool maintained contact with component to a higher depth when the squeeze factor is reduced from 1 to 0.9. Further reduction of squeeze factor to 0.85 resulted in lower fracture depth compared to squeeze factor of 1 and 0.9. Squeezed tool path strategy ensured the support tool contact but not accuracy. Malhotra et al. [28] used in-to-out tool path rather than out-to-in to maintain continuous contact of support tool and termed it as accumulative double sided incremental forming (ADSIF). Using ADSIF, maximum deviation of measured profile to that of ideal profile in case of conical geometry having opening diameter of 60 mm is reported as 1.15 mm. Xu et al. [30] and Zhang et al. [31] proposed a mixed tool path strategy, i.e., first, the component is formed using ADSIF process (in-to-out tool movement) to ensure support tool contact and followed by DSIF process (out-to-in tool movement) with squeeze factor to improve the accuracy. Using this strategy they formed a pyramidal component (opening size of 80 mm) with pockets and reported an average deviation of 0.6 mm and maximum deviation of 1 mm while using the squeeze factor of 0.8. Lingam et al. [20] adopted tool and sheet deflection compensation methodology proposed by Asghar et al. [19] to DSIF process. They reported that the support tool had maintained contact with the sheet throughout forming and the force experienced by support tool while forming the wall region is less than 50 N (i.e., no squeezing) when compensated tool path is used. In case of a 60° cone with opening diameter of 70 mm, they reported that the profile deviation reduced from 1.5 mm to 0.4 mm in the wall region, from 1 mm to 0.22 mm in base region when tool and sheet deflections are compensated. While forming complex geometries using DSIF, the role of forming and support tools have to be selected based on which side of the sheet feature is to be formed. To apply compensations appropriately, features of a geometry have to be recognised and their forming sequence has to be decided. Lingam et al. [22] developed a methodology for automatic feature recognition either by splitting and/or joining the multiple surfaces based on feature characteristics (i.e., saddle points, silhouette loops, boundary relations). However, the accuracy of the multiple feature component is affected by the sequence in which the features are formed. Lingam et al. [22] also studied the importance of feature sequencing on the geometrical accuracy of the component by forming various geometries (a cone with an inclined hump, free form geometry with saddle point) in different feature sequences. They concluded that before forming a feature its surrounding features have to be formed to achieve good accuracy. For a free form component with saddle point and having three features, they reported that the component formed using out-to-in sequence has less profile error, i.e., 0.270 mm, whereas in other feature sequences it is 1.150 mm. Lingam et al. [21] proposed a simple methodology to analytically predict the rigid body displacement during ISF by assuming that the material moves normal to the profile in a stage. They formed a 80° wall angle cone (opening size of 60 mm) in four stages and predicted its geometry. Maximum deviation between the predicted depth to that of the measured depth at the center of component is 0.61 mm, 1.4 mm, 1.9 mm, 2.3 mm after 1st, 2nd, 3rd and 4th stages respectively. After considering tool and sheet deflections, the deviations reduced to 0.06 mm, 0.1 mm, 0.38 mm, 0.2 mm respectively. Moreover, Lingam et al. [23] validated the rigid body displacement prediction methodology [23] and importance of feature sequencing [22] by forming free form geometry (opening size of 60 mm) having multiple features (three features). The maximum profile deviation between predicted profile to that of measured profile is below 0.5 mm in case of features formed in out-to-in sequence. Also, the maximum profile deviation between the predicted one and FEA is below 0.350 mm. Reddy et al. [9] demonstrated multi-stage forming methodology to enhance the accuracy of large components. A conical component of opening diameter 250 mm is formed in two stages using same tool path in both the stages. They reported that the maximum profile error was 2.4–1.4 mm after 1st and 2nd stages respectively. Ren et al. [24] used finite element analysis to develop a regression model to predict and compensate the elastic deflection of sheet that occurs during DSIF. They performed finite element analysis by applying different loads at selected locations on the intermediate geometry to get sheet deflection. A regression model is developed from force–deflection data. Axial force on tool during forming was measured and it was used to predict sheet deflection at that instant from the regression model. For conical geometry having opening size of 70 mm, the maximum profile error reduced from 5.7 mm to 1.5 mm by using compensated tool path. Moser et al. [34] performed explicit FE analysis of DSIF of a varying wall angle (maximum 66.7°) geometry and reported that support tool lost contact in both simulation as well as experiments after forming certain depth. Tool maintained contact where the deviation between predicted and measured thickness is less than 50 μm and the deviation is around 150 μm in remaining region where tool is not in contact. Moser et al. [35] studied the influence of in-plane curvature on contact condition of support tool in DSIF of a varying in-plane curvature geometry with constant wall angle using FEA. They reported that support tool steadily lost contact with sheet while approaching concave regions and the process degenerated to SPIF. Ren et al. [29] studied the significance of support tool contact force on geometrical accuracy and formability of the component formed using DSIF. They developed a force control algorithm using position and force feedback. They reported that using displacement control on both the tools, the support tool lost contact during forming and fracture occurred at a depth of 19 mm for a varying wall angle conical component having opening size of 60 mm. Whereas, using force control approach, support tool maintained the contact with sheet throughout forming and also the depth at fracture is increased to 22 mm. To ensure continuous contact, Lu et al. [36] used pneumatic controlled support tool and investigated the material deformation mechanism in DSIF by varying support force. For a varying wall angle conical component (opening size 100 mm), they reported that depth at fracture increased from 20 mm to 30 mm when support force increased from 240 N to 480 N. Ren et al. [37] carried out simulation of DSIF by incorporating machine compliance and analyzed for tool-sheet contact condition and reported that support tool lost contact at a lesser depth with an increase in machine tool compliance. Leem et al. [38] investigated on accuracy of force predictions in the DSIF numerical simulations by incorporating the kinematic hardening as well as machine compliance. They considered the Yoshida–Uemori multi surfaces hardening model (isotropic hardening + kinematic hardening) and Voce isotropic hardening and performed the numerical simulations with and without machine compliance by using both material models using explicit solver. They compared the measured forming forces with numerically predicted forces of both models without considering machine compliance, and reported that Yoshida–Uemori multi surfaces hardening model predicted forces are closer to experimental measured forces.

In SPIF process, absence of support tool results in unwanted bending at component opening [1,14,19,32]. Using DSIF process, bending at component opening is reduced but there is a tendency for support tool to lose contact with sheet during forming and resulting in less accuracy of the formed component. Attempts made to improve the contact condition using squeeze tool path strategy [27,28] ensured the support tool contact but not the accuracy of the formed components. Sheet and tool deflection compensation methodology [20] ensured the support tool contact and also significantly improved the accuracy. However available analytical methods to predict and compensate sheet spring-back uses theory of small deflections [19,20] which is valid only when the

sheet deflections are small compared to its initial thickness. The above mentioned strategies are validated for different geometries having opening size less than 200 mm × 200 mm. While forming components of larger opening, the deflections are expected to be much higher than the thickness. Hence, in the present work, combination of small deflection and membrane theories are used to predict the sheet deflection and it is validated using numerical as well as experimental studies.

2. Methodology

Double sided incremental forming process uses two tools to form the components, one on either side of the sheet. At any instant, one tool will be forming and the other acts as support. Support tool may lose contact with sheet or squeeze the sheet depending on the distance maintained between forming and support tools [11,13,20,27,29]. To ensure proper contact of support tool, distance between contact points of two tools T_1 and T_2 (Fig. 2(a)) should be very close to the sheet thickness at that instant. In the present work, instantaneous sheet thickness is predicted using overlap methodology proposed by Bhattacharya et al. [39], which is proven to predict thickness with less than 4% error [40]. It is well known from literature [14,19,20,26] that sheet and tool deflections due to forming forces, are the main factors for geometrical inaccuracy of the component. Accuracy of components can be enhanced by predicting sheet and tool deflections accurately and applying compensations for them while generating tool path. For estimation of sheet and tool deflections, first instantaneous sheet thickness is predicted using overlap methodology [39], contact area between tool and sheet is predicted using analytical methodology developed by Bansal et al. [40] and then forming forces are estimated using force equilibrium methodology [40]. Asghar et al. [19] and Lingam et al. [20] used theory of small deflections [41] to predict sheet deflection, which is valid only when deflections are much smaller compared to sheet thickness. In the present work, combination of small deflection and membrane theories are used to predict sheet deflection so that the methodology can be used for small as well as large components. Forming tool deflection is estimated by assuming it to be a cantilever. Finally, compensations for the predicted sheet and tool deflections are applied to tool path to enhance the accuracy of components.

2.1. Prediction of thickness and forming forces

Deformed sheet thickness at any instant is predicted using overlap methodology proposed by Bhattacharya et al. [39]. In the overlap methodology, the initial sheet configuration is divided in to number of elements (AB, BC, CD, ⋯) as shown in Fig. 2(b). Some part of the material in ISF gets deformed repeatedly due to overlap. Amount of increase in length of each element during deformation is determined by assuming that the material moves normal to the profile of component in previous tool pass. Deformed sheet thickness is obtained by imposing volume constancy condition between initial and final positions of the elements. Strain values along the principal directions (Fig. 2(c)) are calculated by assuming plane-strain deformation. Equivalent stress is obtained using stress–strain relation of sheet material. By assuming that the sheet material yields according to von-Mises criterion, stress components along principal directions (i.e., thickness (σ_t), meridional (σ_ϕ), circumferential directions (σ_θ)) are obtained as [39,42]

$$\sigma_t = -\frac{2\sigma_{eq}}{\sqrt{3}}\left(\frac{t}{R+t}\right); \qquad \sigma_\phi = \frac{2\sigma_{eq}}{\sqrt{3}}\left(\frac{R}{R+t}\right); \qquad \sigma_\theta = \frac{\sigma_{eq}}{\sqrt{3}}\left(\frac{R-t}{R+t}\right) \tag{1}$$

where σ_{eq} is the equivalent stress, R is tool radius and t is thickness of sheet at any instant. Bansal et al. [40] estimated the tool sheet contact area by integrating the contact perimeter (Fig. 2(d)) in plane perpendicular to tool axis and the same expression is used in the present work, and is given by

$$A = \frac{\pi R}{2}(R + \Delta z) + \frac{\pi R^2}{2(\delta - \alpha)}(\sin\alpha - \sin\delta) \tag{2}$$

where R is tool radius, Δz is incremental depth, α is wall angle, δ is grove angle.

From finite element analysis of SPIF, contact pressure distribution show that the contact area can be approximated as rectangular strip [40,43]. Length of rectangle (l) is estimated as the length of tool–sheet interaction along meridional direction ($l = R(\alpha + \delta)$) and width of rectangle (m) is calculated from the predicted contact area (A), which is given by $m = A/l$. Assuming that the stresses are uniformly distributed over the entire contact zone, force components along thickness (F_t), circumferential (F_θ) and meridional (F_ϕ) directions are obtained as [40]

$$F_t = \sigma_t \mathrm{ml}; \quad F_\theta = \sigma_\theta \mathrm{lt}; \quad F_\phi = \sigma_\theta \mathrm{mt}$$

However, to predict the sheet and tool deflections, the forces acting on the forming tool in the tool coordinate system are required (Fig. 2(c)). Hence, forces are resolved along axial (F_z) and radial directions (F_r), and are given as [40]

$$F_z = F_\phi \sin\alpha + F_\phi \sin\delta + F_t \cos\left(\frac{\alpha - \delta}{2}\right); \qquad F_r = F_\phi \cos\delta + F_t \sin\left(\frac{\alpha - \delta}{2}\right) - F_\phi \cos\alpha \tag{3}$$

2.2. Prediction of tool deflection

Forces acting on the forming tool (i.e., along axial (F_z), radial (F_r) and tangential (F_{tg}) directions) during ISF are as shown in Fig. 3(a). Majority of tool deflection occurs due to radial force (F_r) and deflection due to other forces can be neglected [19,20]. In the present work, force acting only in radial direction is considered for tool deflection prediction. Tool is assumed as a cantilever with force (F_r) acting at its tip as shown in Fig. 3(b). Forming tool has two parts, tool extension and tool shank. Hence, tool is divided in to two parts of different cross sections and tool deflection is calculated using the moment-area method. Tool deflection at tool tip location is obtained as

$$\delta_t = -F_r\left(\frac{L_1^3}{3EI_1} + \frac{L_1L_2(2L_1 + L_2)}{2EI_2} + \frac{L_2^2(3L_1 + 2L_2)}{6EI_2}\right) \tag{4}$$

where δ_t is tool deflection, E is Young's Modulus of tool material, I_1 and I_2 are moment of inertia and L_1, L_2 are lengths of tool shank and tool extension.

2.3. Prediction of sheet deflection

In ISF process, peripherally clamped sheet is deformed using simple tools moving in a predefined paths. When the tool moves from point A to diametrically opposite location B, profile of components undergoes elastic recovery (point A moves to A') as shown in Fig. 4(a). When the tool is retracted after forming, global elastic recovery takes place (point A' moves to A'') as shown in Fig. 4(a). To predict the elastic deflection of sheet, the loading condition at any instant is considered to be analogous

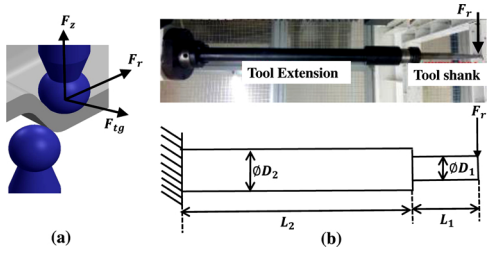

Fig. 3. (a) Forces acting on forming tool, (b) tool shank and its extension assumed as cantilever.

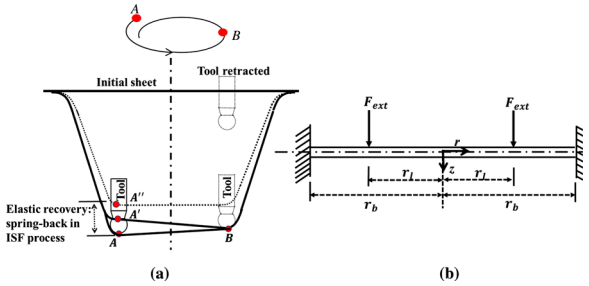

Fig. 4. (a) Schematic showing the spring-back in ISF process, (b) schematic showing the loading condition and parameters used for prediction of sheet deflection.

to concentrically loaded circular sheet clamped along its periphery as shown in Fig. 4(b). In experimental setup, sheet is rigidly fixed along its periphery between two circular clamping plates one each on either side of the sheet (Fig. 11(c)). Adequate number of holes are drilled along the sheet periphery for clamping the sheet to arrest all DOF of sheet edge.

Methodology available in literature [19,20] to predict sheet deflection in ISF used theory of small deflections (neglecting the strains in middle plane of sheet) and is valid only when sheet deflections (w) are small compared to thickness (t_0). For large components, sheet deflection will become higher, hence, influence of membrane force due to stretching has to be considered [41,44] to predict sheet deflection. In the present work, combination of small deflection and membrane theories are used for sheet deflection prediction.

It is well known that applied transverse load (F_{ext}) will deflect the sheet against bending, shearing and membrane stresses. For a transverse deflection of w at a distance η (Fig. 4(b)), some part of the applied load (F_{ext1}) will be balanced by bending and shearing stresses and remaining part (F_{ext2}) will be balanced by membrane stresses [41]. Hence F_{ext1} and F_{ext2} will be functions of w; assuming $F_{ext1} = f_1(w)$ and $F_{ext2} = f_2(w)$, total external force will be

$$F_{ext} = F_{ext1} + F_{ext2} = f_1(w) + f_2(w) \tag{5}$$

Sheet deflection is obtained by solving above expression using predicted axial force as F_{ext}. Methodology to obtain $f_1(w)$ and $f_2(w)$ is explained below using small deflection and membrane theories respectively.

2.3.1. Theory of small deflections

Transverse deflection (w) of a clamped circular sheet due to concentric line load (F_{ext1}) acting at a distance ($r = \eta$) from the center (Fig. 5) can be obtained as [41]

$$F_{ext1} = \frac{4\mathrm{D}w}{\eta\left[(r^2 + r_l^2)\ln\left(\frac{r}{r_b}\right) + \left(\frac{r_b^2 - r^2}{2}\right)\left(1 + \frac{r_l^2}{r_b^2}\right)\right]} \tag{6}$$

where D is the bending rigidity of the sheet $\left(D = \frac{\mathrm{Et}_0^3}{12(1-\nu^2)}\right)$, t_0 is initial sheet thickness, E is Young's modulus, ν is Poisson's ratio, r_b is blank size, η distance from center at which load is acting. Here, material is assumed to be isotropic and strain in middle plane of sheet is neglected.

2.3.2. Membrane theory

It is well known that, if transverse deflection of sheet (w) increases beyond thickness of sheet (t_0), then sheet tends to stretch resulting in membrane stresses [44]. For a circular sheet with concentric line load (F_{ext2}) shown in Fig. 6(a), displacement in radial direction (u) can be neglected [45] because of its symmetry. Hence, strain in tangential direction becomes negligible ($\varepsilon_{tan} = u/r = 0$). Free body diagram of an element at a distance r from the center of sheet is shown in Fig. 6(b). For an element at a radial distance of r from the center (Fig. 6(b)), strain in radial direction can be expressed as [45]

$$\varepsilon_{rad} = \frac{\mathrm{du}}{\mathrm{dr}} + \frac{1}{2}\left(\frac{\mathrm{dw}}{\mathrm{dr}}\right)^2 = \frac{1}{2}\left(\frac{\mathrm{dw}}{\mathrm{dr}}\right)^2 \tag{7}$$

Using Hook's law, membrane force along radial direction (F_{rad}) can be expressed as [45]

$$F_{rad} = \frac{\mathrm{Et}_0}{1-\nu^2}(\varepsilon_{rad} + \nu\varepsilon_{tan})) = C(\varepsilon_{rad}) \tag{8}$$

where C is in-plane rigidity of the sheet $\left(C = \frac{\mathrm{Et}_0}{1-\nu^2}\right)$, t_0 is initial sheet thickness, E is Young's modulus, ν is Poisson's ratio. Applied load (F_{ext2}) will be balanced by the in-plane forces that act along radial and tangential directions. Radial stretching force per unit length acting tangential to deflected surface (Fig. 6(c)) can be resolved into two components, one along out-of-plane (F_{op}) and other along in-plane (F_{ip}) direction of sheet. If transverse load (F_{ext2}) is applied at a distance η from center, then the relation between transverse deflection (w) and out-of-plane force component (F_{op}) is obtained by considering the equilibrium of region of sheet within radius r as shown in Fig. 6(c), and it can be expressed as

$$F_{op} = F_{rad}\frac{\mathrm{dw}}{\mathrm{dr}} \tag{9}$$

Force equilibrium of an element at radius r (where $r > \eta$) in the out-of-plane direction as shown in Fig. 6(b) can be obtained as

$$(F_{op})(r)d\theta = (F_{ext2})(\eta)d\theta \tag{10}$$

where η is the distance from center of sheet at which concentric line load (F_{ext2}) is applied. Governing equation for a peripherally clamped sheet subjected to concentric line load as shown in Fig. 6(a) is obtained by substituting Eq. (8) and Eq. (9) in Eq. (10) as

$$\frac{\mathrm{dw}}{\mathrm{dr}} = \sqrt[3]{\frac{2(F_{ext2})(\eta)}{C}}(r)^{\frac{-1}{3}} \tag{11}$$

For a circular sheet clamped along edge $r = r_b$ as shown in Fig. 6(c), the boundary conditions are

$$w = 0; \qquad \frac{\mathrm{dw}}{\mathrm{dr}} = 0 \quad \text{at } r = r_b \tag{12}$$

After integrating Eq. (11) using above boundary conditions, transverse deflection (w) of sheet can be obtained as

$$w = \frac{3}{2}\sqrt[3]{\frac{2(F_{ext2})(\eta)}{C}}\left(r^{\frac{2}{3}} - r_b^{\frac{2}{3}}\right) \tag{13}$$

where r_b is the distance from the center of sheet at which it is clamped. Above equation can be rewritten as

$$F_{ext2} = \frac{8w^3C}{54\eta\left(r^{\frac{2}{3}} - r_b^{\frac{2}{3}}\right)^3} \tag{14}$$

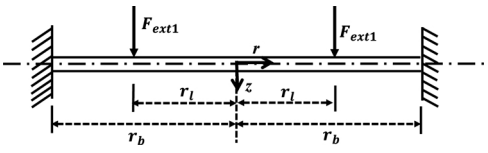

Fig. 5. Schematic of parameters used for sheet deflection prediction.

2.3.3. Combining theories

In incremental sheet forming process, a wide range of sheet sizes are used to form the components. Hence, neither theory of small deflections not membrane theory is applicable in all cases. Combination of small deflection and membrane theories used by Timoshenko [41] to predict the deflection of a peripherally clamped rectangular thin plate subjected to uniformly distributed load. In the present work, above methodology [41] is adopted to find the deflection of peripherally clamped sheet subjected to concentric line load. Total load (F_{ext}) to

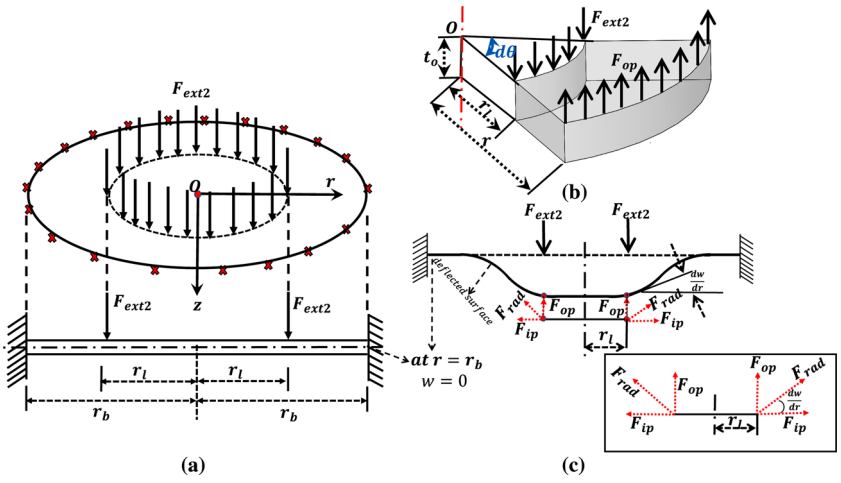

Fig. 6. Clamped circular sheet subjected to line load F_{ext2}. (a) Schematic of parameters used for sheet deflection prediction, (b) free body diagram of element at distance η from center, (c) schematic showing the relationship between force (F_{op}) and deflection (w).

balance the bending, shearing and membrane stresses can be obtained by adding Eqs. (6) and (14).

$$F_{\text{ext}} = \frac{8w^3C}{54\eta\left(r^{\frac{2}{3}} - r_b^{\frac{2}{3}}\right)^3} + \frac{4\text{Dw}}{\eta\left[(r^2 + r_l^2)\ln\left(\frac{r}{r_b}\right) + \left(\frac{r_b^2 - r^2}{2}\right)\left(1 + \frac{r_l^2}{r_b^2}\right)\right]} \tag{15}$$

Contact pressure distribution in incremental forming observed in finite element analysis show that the contact area can be approximated as a rectangular strip [40,43]. Calculation of length and width of rectangular strip is presented in above section (refer Section 2.2). Assuming that the axial load (F_z) predicted at an instance is uniformly distributed along the periphery of the tool-sheet contact area (Fig. 7), concentric line load (F_{ext}) acting on the sheet at distance η is estimated as $F_{\text{ext}} = \frac{\text{Fz}}{2(l+m)}$ and the above Eq. (15) can be rewritten as

$$\frac{F_z}{2(l+m)} = \frac{8w^3C}{54\eta\left(r^{\frac{2}{3}} - r_b^{\frac{2}{3}}\right)^3} + \frac{4\text{Dw}}{\eta\left[(r^2 + r_l^2)\ln\left(\frac{r}{r_b}\right) + \left(\frac{r_b^2 - r^2}{2}\right)\left(1 + \frac{r_l^2}{r_b^2}\right)\right]} \tag{16}$$

Solving the above equation will result in one real root and a conjugate pair. The real root is taken as the transverse deflection (w) of sheet. Procedure to predict sheet deflection in incremental forming is explained using the flow chart presented in Fig. 8.

2.4. Measurement of machine tool error

Two spindles/tools traverses on lead screws mounted on machine frame and results in change in loading location on lead screws leading to different deflections/errors at different locations. Although the tools are programmed to move from one location to other with respect to standard reference plane, there is a relative displacement in tool axial direction. Machine's spindles are programmed to move to various discrete locations of grid within sheet reference plane (x, y) and relative deviation in z direction corresponding to each location is measured

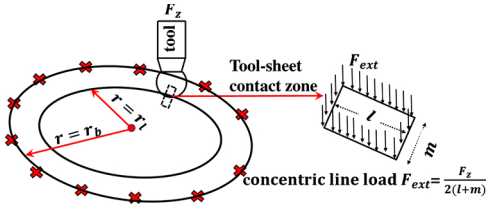

Fig. 7. Schematic showing the loading condition on sheet to predict its deflection using combined theory.

using dial gauge. Similarly, machine tool components deflection/errors in different planes on either side of the sheet reference plane are also measured. An empirical model relating machine tool error and spatial coordinates is developed using the measured data to generate compensated tool path [46].

2.5. Compensated tool path generation

Slicing the surface model (representing the component surface towards the positive z-axis) gives the contact point T1 (between tool-1 and sheet) shown in Fig. 9a. Ideal tool path to form the components is generated by slicing the CAD model of the geometry. Surface models of the geometry are used for slicing by considering it as the surface of the component towards the positive z-axis. Choosing the tip points (P_1, P_2 shown in Fig. 9) as the reference points on tools their ideal locations are obtained by applying tool radius and sheet thickness compensations to the sliced points using the normals at those points. Ideal tool tip locations are obtained as

$$P_1 = T_1 + R_1(\hat{n} - \hat{k}) \tag{17}$$

$$P_2 = T_1 - (R_2 + t_f)\hat{n} + R_2\hat{k} \tag{18}$$

where $\hat{n}$ is the unit normal at contact point (T_1), $\hat{k}$ is the normal along tool axis, t_f is sheet thickness, R_1 is radius of tool-1 and R_2 is radius of tool-2. Tool deflection and sheet spring-back have to be compensated to enhance the accuracy of the components. Forming tool deflects because of the forces acting on it, whereas, the support tool will not deflect significantly as the force applied by it is very less (below 50 N of force is measured during forming). Sheet deflection effect the location of both the tools as both the contact points (T_1, T_2) will undergo spring-back when the tools move away from them. Hence, tool deflection compensation is applied only to the forming tool and sheet deflection compensation is applied to both the tools. Fig. 9 illustrates the tool and sheet deflection compensation when tool-1 is forming tool. In this case tool tip locations are obtained as

$$P_{1C} = P_1 - \delta_t(n_x + n_y) - w(n_z) \tag{19}$$

$$P_{2C} = P_2 + w(n_z) \tag{20}$$

If tool-2 is forming tool then tool tip locations are obtained as

$$P_{1C} = P_1 - w(n_z) \tag{21}$$

$$P_{2C} = P_2 + \delta_t(n_x + n_y) + w(n_z) \tag{22}$$

where P_{1C} or P_{2C} is the forming tool tip point locations after applying sheet and tool deflection compensations, n_x, n_y, n_z are the components

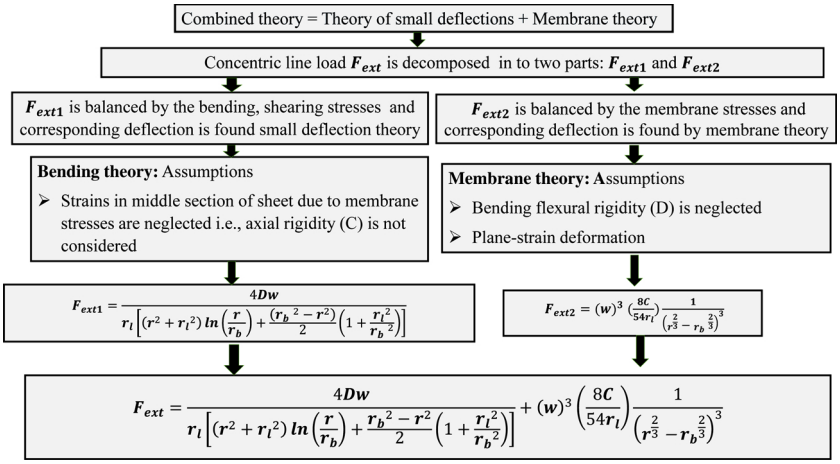

Fig. 8. Flow chart to predict sheet deflection.

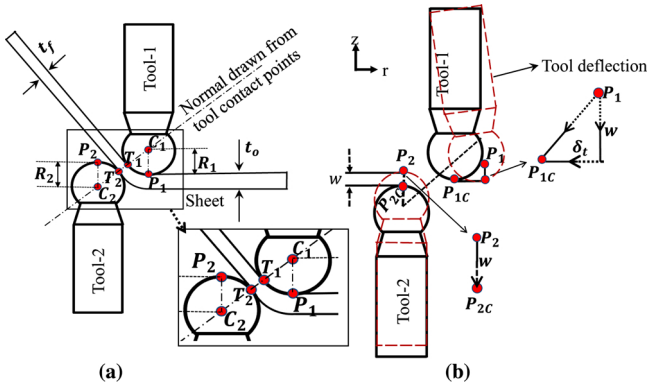

Fig. 9. Schematic showing compensation methodology applied to forming and support tools. (a) Tool radius and sheet thickness compensation, (b) tool and sheet deflection compensation.

of outward normal at contact point, δ_t is tool deflection, w is sheet deflection.

After applying the compensations for tool path, it was observed that there is an increase in forming forces due to increased wall angle. Therefore, sheet and tool deflections are recalculated iteratively using the increased wall angle. In the first iteration itself; it is found that the increase in deflection is close to 20 μm (60° cone, incremental depth of 0.5 mm, tool diameter of 12.7 mm). Hence, only one iteration is used to obtain the compensated tool path.

3. Results and discussion

In incremental sheet forming, sheet and tool deflections are the main factors for geometrical errors. It is well known that if the feature being formed is close to the fixture, then majority of the external load is balanced by bending stresses and sheet deflections will be smaller than thickness. However, for features that are far from fixture opening, sheet deflection will be much higher than thickness. Earlier attempts [19,20] to predict sheet deflection used small deflection theory and is valid only when the deflections are small compared to thickness. In the present work, a methodology applicable for small as well as large components (formed using either small or large sheet) is developed by combining small deflection and membrane theories. Predictions of developed methodology are validated by comparing with FEA predictions and experimental measurements performed during the present work. Aluminium (Al8011) sheet of 0.8 mm thickness, tool diameter of 12.7 mm and incremental depth of 0.5 mm are chosen for validation. The stress–strain relation of sheet material is $\sigma = 144(\varepsilon)^{0.02}$ MPa.

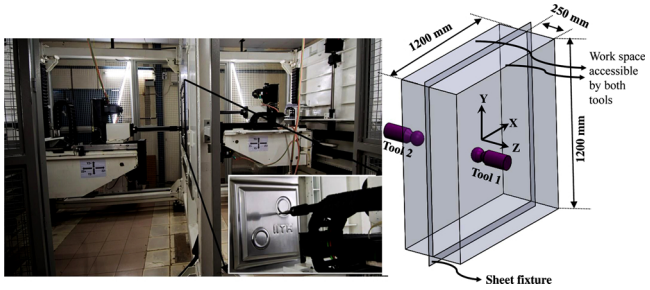

Fig. 10. Custom designed DSIF machine (IIT-Hyderabad).

Components are formed using a custom built DSIF machine shown in Fig. 10 and it consists of two independently controlled spindles and are operated using SIEMENS 840D controller. Tool path is developed in such a way that; the two tools traverse in a synchronized manner during forming. In DSIF, support tool has to maintain continuous contact with sheet throughout forming with a minimal force to avoid squeezing. Profiles of the formed components are measured using gantry type Coordinate Measuring Machine (CMM, resolution 0.1 μm) after unclamped from the fixture.

3.1. Validation

Sheet deflection predicted using proposed methodology is validated using finite element analysis (FEA) and measured values. During the forming process, local and global spring-back of sheet takes place. Local spring back is the elastic recovery of sheet when the tool moves away from the point and the global spring back is the elastic recovery when the tool is retracted. Total spring back (local + global) will be equal to the elastic deflection (Fig. 11(a)) of sheet due to forming forces. Hence, to validate the proposed methodology, deflection predictions are compared with numerical and experimental predictions. An elastic finite element analysis is carried out using ABAQUS for a circular sheet fixed along its periphery. Sheet is modeled as deformable body and is discretized using four noded quadratic shell elements (S4R) of size 1 mm. Mesh convergence study is carried out by predicting sheet deflection using mesh sizes of 8 mm, 4 mm, 2 mm, 1 mm, 0.5 mm. It is observed that the variation of sheet deflection is below 1 μm when mesh size changes from 2 mm to 1 mm. Hence, 1 mm mesh size is chosen for FE analysis. Tool with spherical head of 12.7 mm in diameter is modeled as analytical rigid. For tool, rotational DOF as well as translation in x and y directions are arrested. Interaction between tool and sheet is modeled as frictionless surface-to-surface contact as sheet is well lubricated. Axial force F_z (in z-direction) is applied on the tool

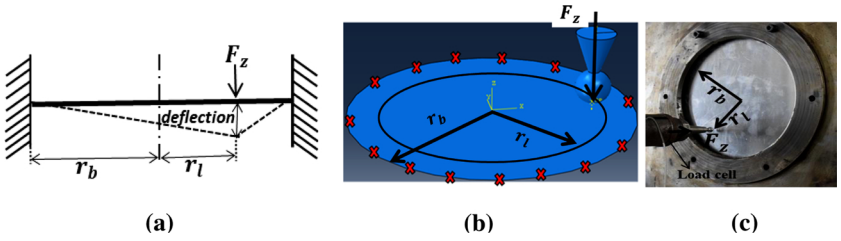

Fig. 11. (a) Loading condition in ISF, (b) FEA model, (c) experimental measurement.

Table 1
Comparison of sheet deflections predicted using small deflection theory, combined theory, FEA and experimental measurement.

Sheetsize r_b (mm)	Loading location r_l (mm)	Small deflection theory (mm)	Combined theory (mm)	FEA (mm)	Experimental measurement (mm)
50	42	0.51	0.428	0.46	0.49
350	300	263.2	4.05	4.18	4.5
1000	900	1427	7.95	7.2	Not performed due to machine size restrictions

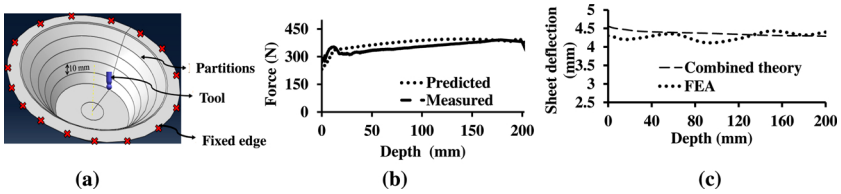

Fig. 12. (a) Varying wall angle geometry modeled to a depth of 50 mm, (b) comparison of measured and predicted axial forces, (c) sheet deflection variation with depth.

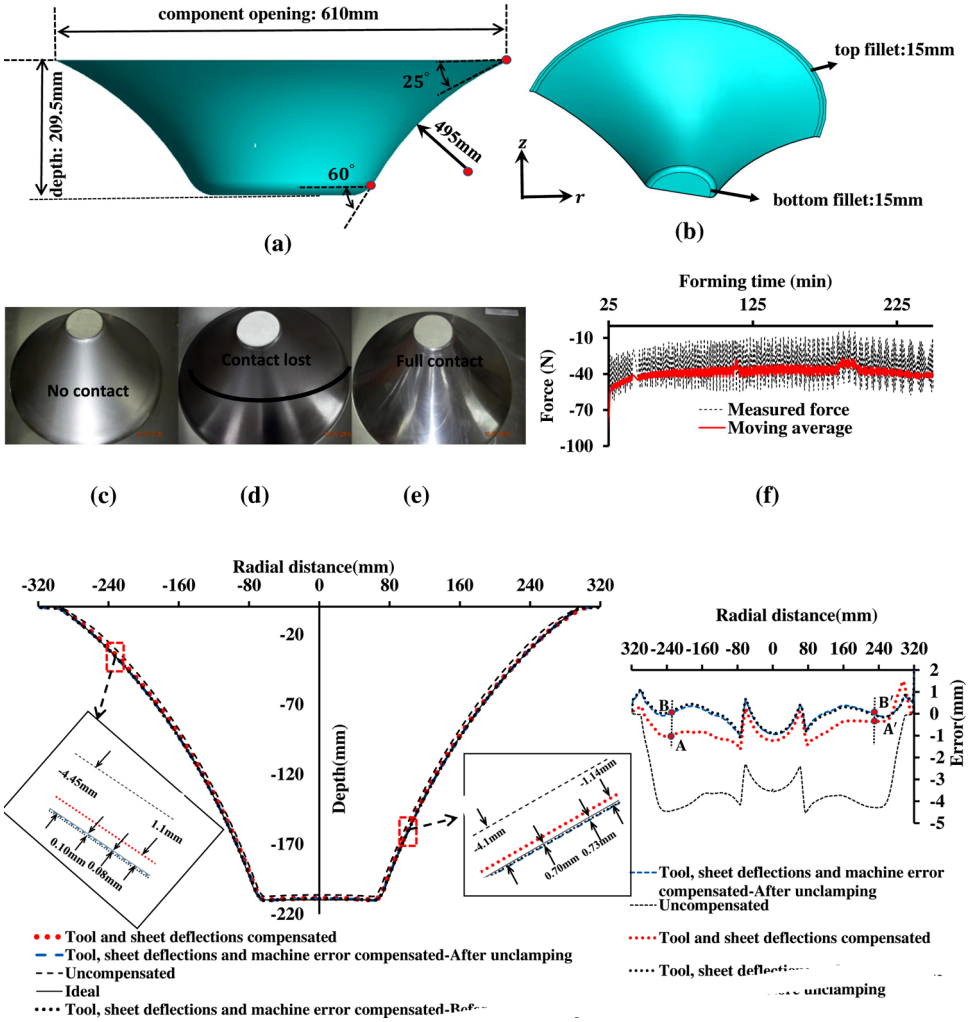

Fig. 13. Varying wall angle component with 610 mm opening diameter (a), (b) CAD model and geometrical parameters, (c) no compensations, (d) sheet and tool deflections compensated, (e) sheet, tool deflections and machine tool error compensated, (f) axial force on support tool, (g) profile comparisons, (h) profile error.

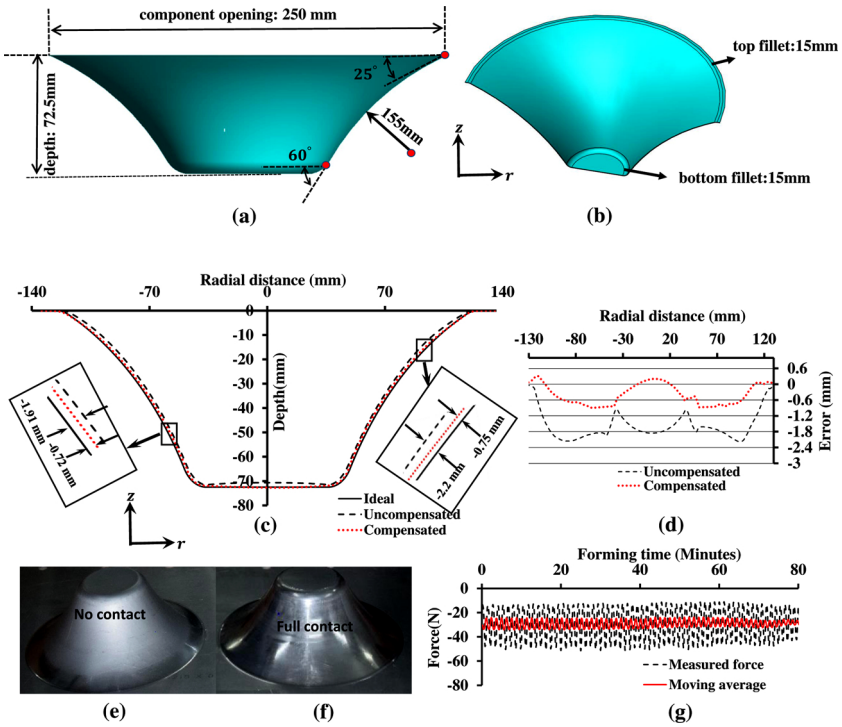

Fig. 14. Varying wall angle component with 250 mm opening diameter (a), (b) CAD model and geometrical parameters, (c) profile comparisons, (d) profile error, (e) component formed using uncompensated tool path, (f) component formed using compensated tool path, (g) axial force on support tool.

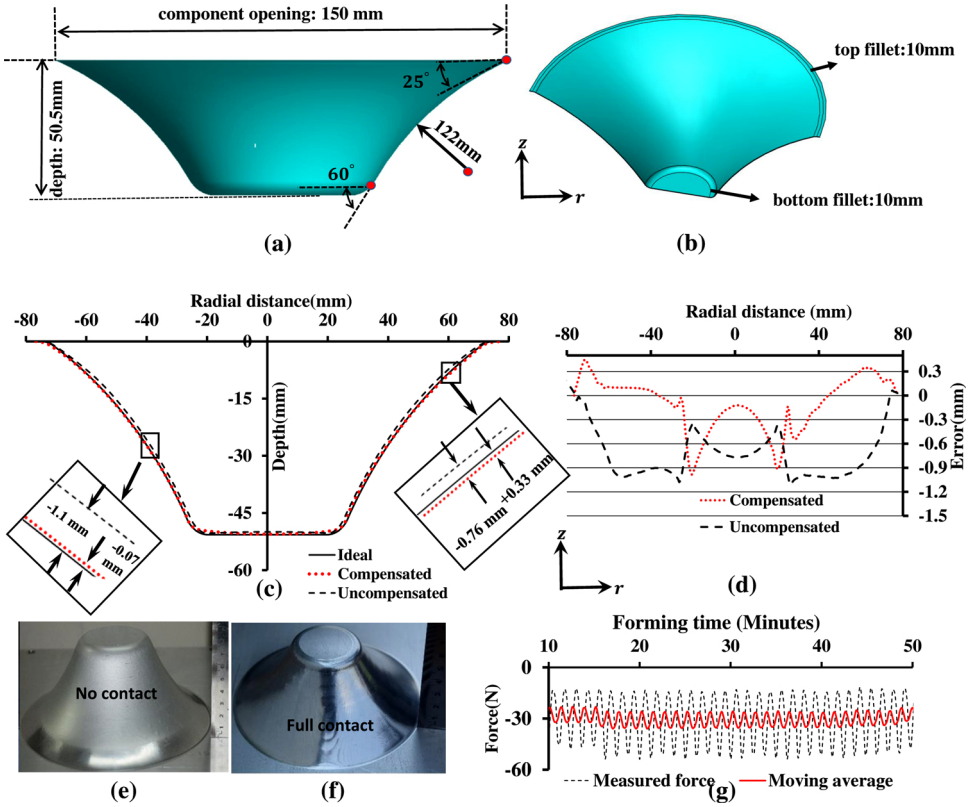

Fig. 15. Varying wall angle component with 150 mm opening diameter (a), (b) CAD model and geometrical parameters, (c) profile comparisons, (d) profile error, (e) component formed using uncompensated tool path, (f) component formed using compensated tool path, (g) axial force on support tool.

placed at a radius of r_l as shown in Fig. 11(b). Axial force predicted using force equilibrium method is used for FE analysis. Displacement of sheet in axial direction exactly below the tool, is taken as the sheet deflection. In experimental measurement, force is measured using a single component load cell mounted on the tool (Fig. 11(c)). Forming tool is moved in steps of 5 μm till the reaction force on the tool reached 381 N and its displacement from initial sheet surface is taken as the sheet deflection. Comparison of sheet deflection predictions for small as

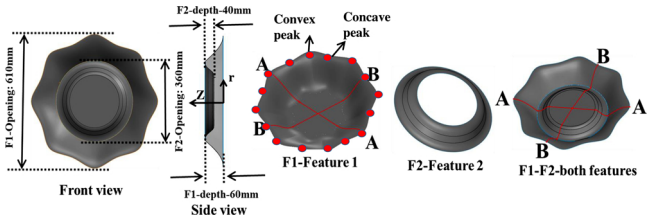

Fig. 16. CAD model and geometric parameters of free form geometry with two features.

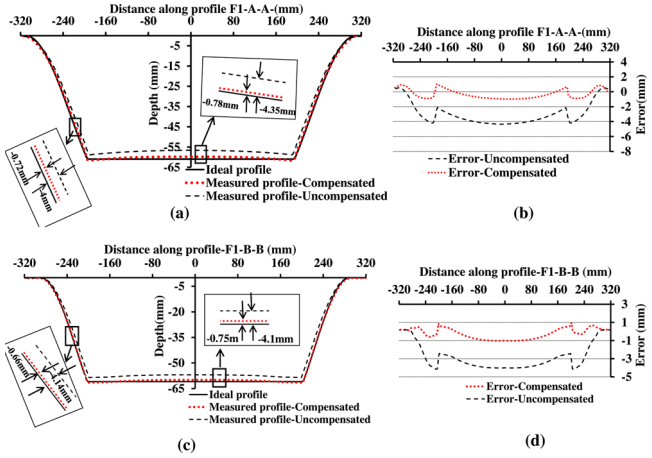

Fig. 17. Feature F1 of free-form geometry with 610 mm opening diameter, (a) profile comparison along section AA, (b) error along section AA, (c) profile comparison along section BB, (d) error along section BB.

well as large size sheets (radius 50 mm, 350 mm, 1000 mm) is shown in Table 1. For small sheet (50 mm radius), the deflection is less than its thickness and both the theories predicted approximately same deflection as that of FEA and experiment. However, for large sheet, deflection is higher than thickness and prediction using theory of small deflections is very high. Whereas, combined theory predicted the deflection with less than 10% error from FEA predictions and experimental measurements. Measurement of tool deflection is carried out by applying known loads at close to tool-tip and deflection is measured using dial gauge. The variation in predicted and measured tool deflections are within 10 μm.

A truncated conical component with wall angle varying from 25° to 60°, opening diameter of 610 mm is chosen to validate the effectiveness of force prediction methodology (Fig. 12(a)). Forming force is predicted at any location using methodology proposed by Bansal et al. [40]. Forming force in this geometry varies continuously as it depends on local wall angle. Fig. 12(b) shows the comparison of measured and predicted forming force (F_z) and they are in very good agreement. For a flat circular sheet clamped along its periphery (Fig. 11(c)), as the loading location moves away from the fixed boundary, deflection of sheet will increase due to lower stiffness in that region. However, in ISF, as forming tool moves in an out-to-in tool path, stiffness of the formed region of the sheet will increase which will reduce the deflection. Therefore, combined effect of stiffness is studied using FE analysis. A 600 mm opening diameter varying wall angle cone (25–60°) is modeled at various depths starting from 0 mm (flat sheet) and in steps of 10 mm. At each depth the sheet deflection due to forming force (F_z) is predicted using FE analysis. Thickness of sheet in the formed region is obtained using overlap methodology [39] as it will be varying with wall angle. This is done by dividing the formed region in to regions of 10 mm depth (Fig. 12(a)) and assigning the average predicted thickness of that region. Axial forming force at each depth is obtained by Eq. (3) using the instantaneous wall angle and is applied on the tool (Fig. 12(a)). Maximum variation of sheet deflection with depth (Fig. 12(c)) is found to be 0.3 mm and the maximum error between prediction using combined theory and FEA is 10%. Comparison of sheet deflection predictions of combined theory at different depths with that of FEA for constant wall angle cone (30°, opening diameter 620 mm, fixture size 700 mm, depth 130 mm) as well as pyramid (60°, opening size 430 mm, fixture size 700 mm, depth 180 mm) that are located at centre of clamping region, constant wall angle cone located asymmetrically (45°, opening diameter 200 mm, fixture size 700 mm and located within one of the quadrants of clamping region, depth 60 mm), varying wall angle asymmetrical shallow geometry (maximum and minimum opening sizes 620 mm and 560 mm respectively, depth 75 mm, maximum wall angle 28°, fixture size 700 mm) as well as freeform component that needs to be formed by both the tools with local stiffeners) indicates that the variation is within 10%. Hence, it is assumed that the sheet deflection during ISF remains approximately same throughout the component, and is equal to the deflection calculated at the component opening. In the present case component opening radius of varying wall angle component is 300 mm. Therefore, to predict the deflection of the sheet at any instant during forming, first forming force (F_z) is obtained by using Eq. (3) and sheet deflection due to F_z at a radial distance equal to component opening is obtained by solving Eq. (16).

3.2. Experimental results

A varying wall angle conical component with different opening diameters (i.e., 610 mm, 250 mm and 150 mm) is chosen to validate the proposed methodology for small as well as large components. In addition, a free-form geometry having two features, one symmetric and other asymmetric is also chosen to demonstrate the robustness of deflection compensation methodology. To check the repeatability, three components are formed in each case and profile error of each component are measured. Maximum change in profile error of three components is within 50 μm and average of them is presented. Measured profiles of the components formed using with and without compensated tool paths are compared with ideal profiles and the error between them is presented.

3.2.1. Varying wall angle components

A truncated conical component with wall angle varying from 25° to 60°, opening diameter of 610 mm is formed using compensated as well as uncompensated tool paths. Dimensions of the geometry are as shown in Fig. 13(a) and (b). For the above geometry, predicted sheet deflection is varied from 4.26 mm to 4.56 mm, tool deflection varied from 0.20 mm to 0.35 mm and machine tool error varied from +0.1 mm to −0.27 mm. Using uncompensated tool path, maximum error in the wall region is −4.45 mm and in the base region is −3.53 mm. Note that, negative error indicates under forming and positive error indicates over forming. Fig. 13(c) shows that the support tool lost contact after the fillet region while using uncompensated tool path. Even after compensating for sheet and tool deflections, support tool maintained contact only on one side of the component (Fig. 13(d)) because of machine tool related errors. Hence, machine tool error is measured and compensated by developing an empirical model [46]. The relative displacement between the two tools in axial direction when they move by same distance in xy-plane is taken as the machine tool error (Fig. 10). When machine tool error is compensated along with tool and sheet deflections, the support tool has maintained contact throughout the forming without squeezing the sheet (Fig. 13(e)) and the average force on support tool while forming is 40 N as shown in Fig. 13(f). When machine tool error is not compensated, dimensional error at one of the chosen location (point A shown in Fig. 13(h)) is −1.04 mm and the error at diagonally opposite location of A (A′) is −0.36 mm. After compensating the machine tool error, dimensional error at B is +0.11 mm and at B′ it is +0.09 mm. After compensating for sheet, tool deflections and machine tool errors, maximum error in wall and base regions has reduced to +0.73 mm and −0.77 mm respectively. In

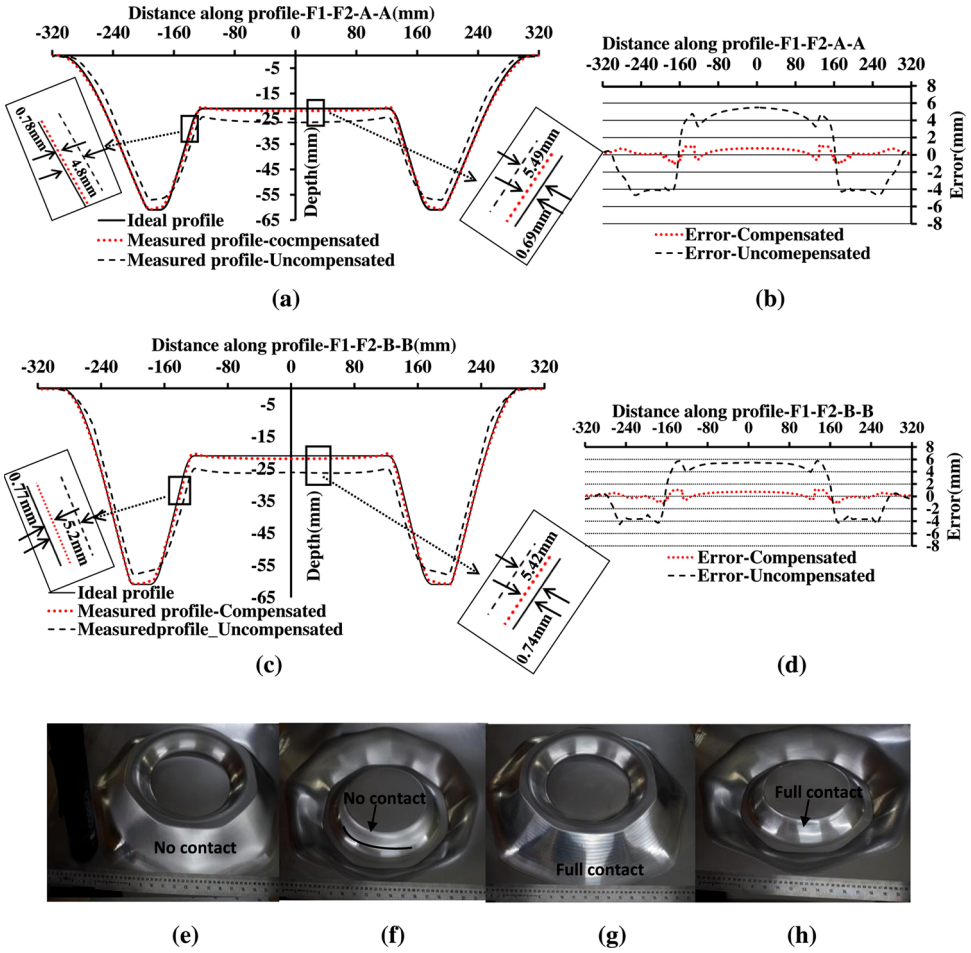

Fig. 18. Features F1 and F2 of free form geometry with 610 mm opening diameter. (a) Profile comparison along section AA, (b) error along section AA, (c) profile comparison along section BB, (d) error along section BB, (e, f) component formed using uncompensated tool path, (g, h) component formed using compensated tool path.

addition, profile variation due to spring-back after unclamping is measured and it is observed that there is an insignificant variation (maximum difference of 30 μm). Maximum error in wall region before unclamping is +0.70 mm and after unclamping is +0.73 mm as shown in Figs 13 (g) and (h). Hence, experimental results presented further are of the components formed using machine tool error compensated tool paths. Hereafter, compensated tool path refers to sheet and tool deflections are compensated, while uncompensated tool paths are generated without deflection compensations. In both the cases machine tool error is compensated.

A truncated conical component with wall angle varying from 25° to 60°, opening diameter of 250 mm is formed using compensated as well as uncompensated tool paths. Dimensions of the geometry are shown in Figs. 14(a) and (b). For the above geometry, predicted sheet deflection is varied from 3.19 mm to 3.45 mm, tool deflection is varied from 0.21 mm to 0.29 mm and machine tool error varied from +0.05 mm to −0.14 mm. Using compensated tool path, the maximum error along the wall region has reduced from −2.2 mm to −0.75 mm (Fig. 14(c)), and in the base region, it is reduced from −1.85 mm to +0.2 mm. Comparison of the measured profiles of the components formed using with and without compensated tool paths are shown in Fig. 14(c) and corresponding errors are shown in Fig. 14(d). Support tool maintained contact throughout depth of the component formed using compensated tool path (Fig. 14(f)). With uncompensated tool path, support tool lost contact after forming fillet region (Fig. 14(e)). Average force on support tool while forming is 30 N and the maximum force is 50 N (Fig. 14(g)).

A truncated conical component with varying wall angle from 25° to 60° with opening diameter of 150 mm is formed using compensated as well as uncompensated tool paths. Dimensions of the geometry are shown in Fig. 15(a) and (b). For the above geometry, predicted sheet deflection is varied from 2.07 mm to 2.23 mm, tool deflection is varied from 0.14 mm to 0.21 mm and machine tool error varied from +0.04 mm to −0.06 mm. Comparison of the measured profiles of the components formed using with and without compensated tool paths is shown in Fig. 15(c) and corresponding errors are shown in Fig. 15(d). Using compensated tool path, maximum error along the wall region has reduced from −1.1 mm to +0.33 mm, and in the base region, it reduced from −0.76 mm to +0.13 mm. When uncompensated tool path is used, support tool lost contact after forming fillet region (Fig. 15(e)). With compensated tool path, support tool maintained contact throughout the forming (Fig. 15(f)). Average force on support tool is 35 N and the maximum force is 50 N (Fig. 14(g)).

3.2.1.1. Free-form geometry with convex and concave features. A free-form geometry with two features (F1, F2) is chosen to demonstrate the applicability of the proposed methodology to asymmetric components (Fig. 16). Forming and supporting role of tools change while forming features F1 and F2. Two features (F1 and F2) in the free-form geometry are recognized by splitting the geometry using planes parallel to initial sheet plane [22]. Opening of feature F1 has convex and concave segments and its wall angle is varying from 0° to 45° (Fig. 16). It is formed using tool that is on the negative z-axis side (T_1), while other (T_2) acted as support tool. Conical feature F2 of wall angle 45° is formed on the base of feature F1. Roles of tools are reversed while forming F2 i.e.,

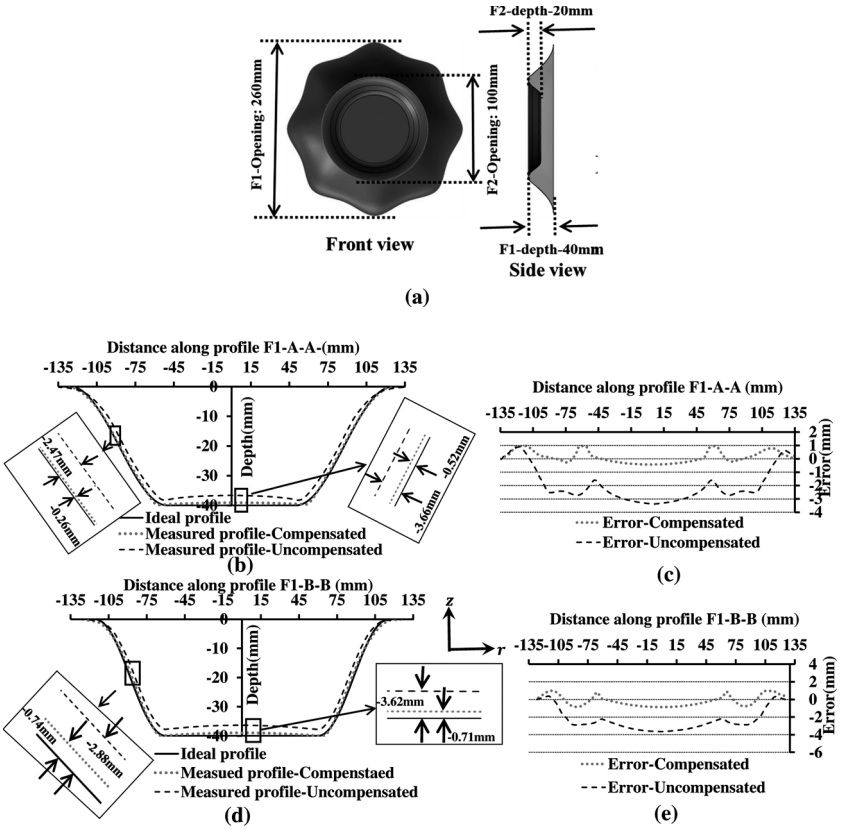

Fig. 19. Feature F1 of free-form geometry with 260 mm opening diameter, (a) CAD model, (b) profile comparison along section AA, (c) error along section AA, (d) profile comparison along section BB, (e) error along section BB.

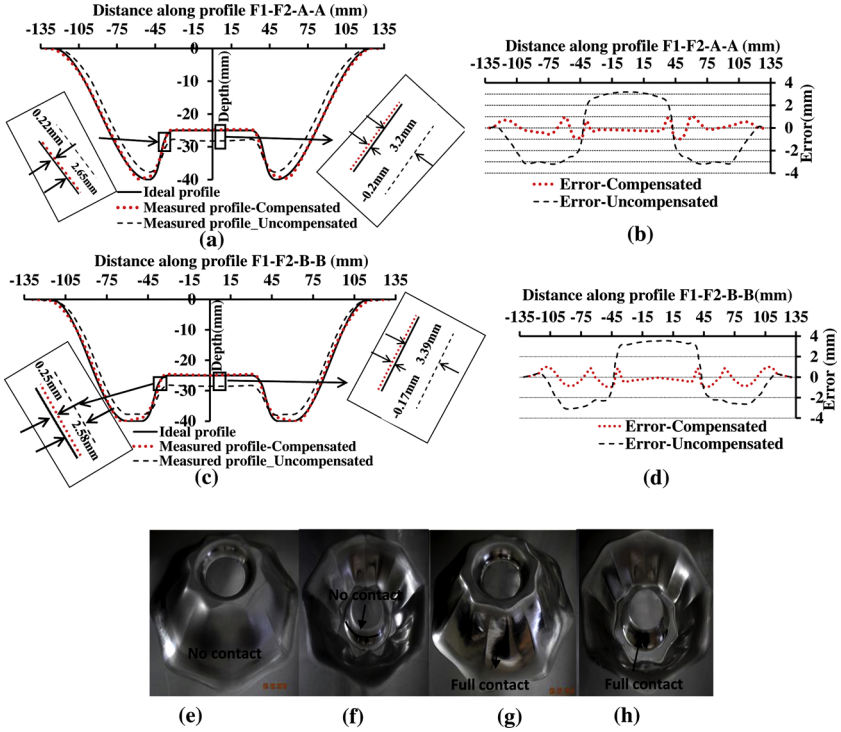

Fig. 20. Features F1 and F2 of free form geometry with 260 mm opening diameter (a) profile comparison along section AA (b) error along section AA (c) profile comparison along section BB (d) error along section BB (e),(f) component formed using uncompensated tool path (g), (h) component formed using compensated tool path.

T2 formed the geometry and T1 provided the support. Deflection compensations are applied to the tools based on their role (either forming or supporting tool).

Feature F1 with component opening of 610 mm and depth of 60 mm (Fig. 16) is formed using compensated as well as uncompensated tool paths. For the above geometry, predicted sheet deflection is varied from 3.2 mm to 5.4 mm, tool deflection is varied from 0.15 mm to 0.3 mm and machine tool error varied from +0.1 mm to −0.28 mm. Profile comparison is carried out along two sections i.e., along A–A and B–B passing through the maximum and minimum radius of opening

respectively (Fig. 16). Comparison of the measured profiles of components formed using with and without compensated tool paths with that of ideal profiles are shown in Fig. 17(a) and (c) and errors between them are shown in figures 17(b) and (d). Note that, for feature F1, positive error means over-forming, while for feature F2, it is under-forming. Using compensated tool path, maximum error along section A-A in the wall region has reduced from −4 mm to −0.72 mm (Fig. 17(b), and in the base region, it is reduced from −4.35 mm to −0.78 mm Along section B–B in the wall region, maximum error reduced from −4.14 mm to −0.66 mm as shown in Fig. 17(d).

Conical feature (F2) with component opening of 360 mm and depth of 40 mm (Fig. 16) is formed on the base of already formed feature F1 using compensated as well as uncompensated tool paths. Comparison of the measured profiles of the components formed using with and without compensated tool paths with that of ideal profiles are shown in Fig. 18(a) and (c) and errors between them are shown in Fig. 18(b) and (d). Using compensated tool path, maximum error along section A–A in the wall region is reduced from 4.8 mm to 0.78 mm and in the base region, it reduced from 5.49 mm to 0.69 mm (Fig. 18(b)). Along section B–B maximum error in wall region reduced from 5.2 mm to 0.77 mm (Fig. 18(d)). When uncompensated tool path is used, support tool has lost contact after forming fillet region (Fig. 18(e) and (f)). While forming with compensated tool path, support tool maintained contact throughout the depth of component (Fig. 18(g) and (h)).

A smaller free-form geometry shown in Fig. 19(a) (similar to the one shown in Fig. 16) is formed to demonstrate the robustness of the prediction methodology. Opening diameter of the component is 260 mm and depth is 40 mm. For the above geometry, predicted sheet deflection is varied from 3 mm to 4.23 mm, tool deflection is varied from 0.15 mm to 0.27 mm and machine tool error varied from +0.05 mm to −0.15 mm. Comparison of the measured profiles of components formed using with and without compensated tool paths with that of ideal profiles are shown in Fig. 19(b) and (d) and errors between them are shown in Fig. 19(c) and (e). Using compensated tool path, maximum error along section A–A in the wall region has reduced from −2.47 mm to −0.26 mm (Fig. 19(c)), while along section B–B it reduced from −2.88 mm to −0.74 mm (Fig. 19(e)).

Conical feature F2 with component opening of 100 mm and depth of 20 mm is formed on the base of the already formed feature F1 using compensated as well as uncompensated tool paths. Comparison of the measured profiles of the components formed using with and without compensated tool paths with that of ideal profiles are shown in Fig. 20(a) and (c) and errors between them are shown in Figs. 20(b) and (d). Using compensated tool path, maximum error along section A–A in the wall region has reduced from 2.65 mm to 0.22 mm (Fig. 20(b)), while along section B–B it reduced from 2.58 mm to 0.25 mm (Fig. 20(d)). When uncompensated tool path is used, support tool has lost contact after forming fillet region (Figs. 20(e) and (f)). While forming with compensated tool path, support tool has maintained contact throughout the depth of component (Figs. 20(g) and (h)).

Tool and sheet deflections are major reasons for inaccuracies in ISF. For small components or features that are close to the fixture, majority of the transverse load is balanced by bending stresses, where membrane effects can be neglected. However, for features that are far from fixture, membrane stresses will significantly resists the applied transverse load. In the present work, combination of small deflection and membrane theories is used to predict the sheet deflection. In this way all the stresses in the sheet are considered simultaneously in sheet deflection prediction, making the methodology suitable for small as well as large deflections. In addition, machine tool related errors are reduced using an empirical model developed during present work. Two different geometries (varying wall angle axisymmetric, asymmetric with maximum opening size of 610 mm) are formed with maximum error less than 800 μm using compensated tool paths generated using the proposed methodology.

4. Conclusions

Sheet and tool deflections are significant factors for geometrical errors in the components formed using double sided incremental forming. When the sheet deflection is less than its thickness, theory of small deflections can be used to predict sheet deflection. However, for features that are far from fixture opening and large components, sheet deflection will be much higher than thickness. In the present work, a methodology is developed to predict and compensate sheet deflections using combination of small deflection and membrane theories. In addition, machine tool errors are measured and an empirical model is developed to compensate the errors that ensured the support tool contact throughout the forming. Applicability of developed methodology to small as well as large components is demonstrated using numerical and experimental validation. Sheet deflection predicted using proposed methodology is within 10% error compared to finite element predictions and measured values. Varying wall angle axisymmetric components of three different openings (opening diameters 150 mm, 250 mm, 610 mm) and a free-form component of two different openings (component opening 260 mm, 610 mm) are formed with maximum error less than 800 μm using compensated tool paths.

Declaration of Competing Interest

The authors report no declarations of interest.

Acknowledgment

This work is supported by SERB, Department of Science and Technology, New Delhi, India (Sanction no. EMR/2015/000286).

References

[1] Jeswiet J, Micari F, Hirt G, Bramley A, Duflou J, Allwood J. Asymmetric single point incremental forming of sheet metal. CIRP Annals 2005;54(2):88–114.
[2] Cao J, Huang Y, Reddy N, Malhotra R, Wang Y. Incremental sheet metal forming: advances and challenges. Proc ICTP 2008 Int Conf Technol Plasticity. 2008. p. 751–2.
[3] Bambach M, Araghi BT, Hirt G. Strategies to improve the geometric accuracy in asymmetric single point incremental forming. Prod Eng 2009;3(2):145–56.
[4] Emmens W, Sebastiani G, van den Boogaard AH. The technology of incremental sheet forming – a brief review of the history. J Mater Process Technol 2010;210(8):981–97.
[5] Reddy NV, Lingam R, Cao J. Incremental sheet metal forming processes. Handbook of manufacturing engineering and technology Springer; 2015. 2014. p. 411–52.
[6] Behera AK, de Sousa RA, Ingarao G, Oleksik V. Single point incremental forming: an assessment of the progress and technology trends from 2005 to 2015. J Manuf Process 2017;27:37–62.
[7] Gatea S, Ou H, McCartney G. Review on the influence of process parameters in incremental sheet forming. Int J Adv Manuf Technol 2016;87(1–4):479–99.
[8] Duflou JR, Habraken A-M, Cao J, Malhotra R, Bambach M, Adams D, et al. Single point incremental forming: state-of-the-art and prospects. Int J Mater Forming 2018;11(6):743–73.
[9] Reddy NV, Lingam R. Double sided incremental forming: capabilities and challenges. J Phys: Conf Ser 2018;1063:012170.
[10] Lu H, Liu H, Wang C. Review on strategies for geometric accuracy improvement in incremental sheet forming. Int J Adv Manuf Technol 2019:1–37.
[11] Peng W, Ou H, Becker A. Double-sided incremental forming: a review. J Manuf Sci Eng 2019;141(5):050802.
[12] Wang H, Zhang R, Zhang H, Hu Q, Chen J. Novel strategies to reduce the springback for double-sided incremental forming. Int J Adv Manuf Technol 2018;96(1–4):973–9.
[13] Meier H, Buff B, Laurischkat R, Smukala V. Increasing the part accuracy in dieless robot-based incremental sheet metal forming. CIRP Annals 2009;58(1):233–8.
[14] Ambrogio G, Costantino I, De Napoli L, Filice L, Fratini L, Muzzupappa M. Influence of some relevant process parameters on the dimensional accuracy in incremental forming: a numerical and experimental investigation. J Mater Process Technol 2004;153:501–7.
[15] Hirt G, Junk S, Bambach M, Chouvalova I. Process limits and material behaviour in incremental sheet forming with CNC-tools. Materials Science Forum, Vol. 426. Zurich-Uetikon, Switzerland: Trans Tech Publications Ltd; 2003. p. 3825–30.
[16] Ambrogio G, Cozza V, Filice L, Micari F. An analytical model for improving precision in single point incremental forming. J Mater Process Technol 2007;191(1–3):92–5.
[17] Behera AK, Verbert J, Lauwers B, Duflou JR. Tool path compensation strategies for

single point incremental sheet forming using multivariate adaptive regression splines. Computer-Aided Des 2013;45(3):575–90.
[18] Allwood JM, Music O, Raithathna A, Duncan SR. Closed-loop feedback control of product properties in flexible metal forming processes with mobile tools. CIRP Annals 2009;58(1):287–90.
[19] Asghar J, Lingam R, Shibin E, Reddy NV. Tool path design for enhancement of accuracy in single-point incremental forming. Proc Inst Mech Engrs, Part B: J Eng Manuf 2014;228(9):1027–35.
[20] Rakesh L, Amit S, Reddy NV. Deflection compensations for tool path to enhance accuracy during double-sided incremental forming. J Manuf Sci Eng 2016;138(9):091008.
[21] Lingam R, Bansal A, Reddy NV. Analytical prediction of formed geometry in multi-stage single point incremental forming. Int J Mater Forming 2016;9(3):395–404.
[22] Lingam R, Prakash O, Belk J, Reddy N. Automatic feature recognition and tool path strategies for enhancing accuracy in double sided incremental forming. Int J Adv Manuf Technol 2017;88(5–8):1639–55.
[23] Lingam R, Bansal A, Prakash O, Venkata Reddy N. Mechanics-based integrated product and process design for incremental forming. J Manuf Sci Eng 2018;140(2):021016–21.
[24] Ren H, Xie J, Liao S, Leem D, Ehmann K, Cao J. In-situ springback compensation in incremental sheet forming. CIRP Annals 2019;1936:1–4.
[25] Duflou J, Callebaut B, Verbert J, De Baerdemaeker H. Laser assisted incremental forming: formability and accuracy improvement. CIRP Annals 2007;56(1):273–6.
[26] Duflou J, Callebaut B, Verbert J, De Baerdemaeker H. Improved spif performance through dynamic local heating. Int J Machine Tools Manuf 2008;48(5):543–9.
[27] Malhotra R, Cao J, Ren F, Kiridena V, Cedric Xia Z, Reddy N. Improvement of geometric accuracy in incremental forming by using a squeezing toolpath strategy with two forming tools. J Manuf Sci Eng 2011;133(6):061019-1–1.
[28] Malhotra R, Cao J, Beltran M, Xu D, Magargee J, Kiridena V, et al. Accumulative-DSIF strategy for enhancing process capabilities in incremental forming. CIRP Annals 2012;61(1):251–4.
[29] Ren H, Li F, Moser N, Leem D, Li T, Ehmann K, et al. General contact force control algorithm in double-sided incremental forming. CIRP Annals 2018;67(1):381–4.
[30] Xu R, Ren H, Zhang Z, Malhotra R, Cao J. A mixed toolpath strategy for improved geometric accuracy and higher throughput in double-sided incremental forming. ASME 2014 international manufacturing science and engineering conference co-located with the JSME 2014 international conference on materials and processing and the 42nd North American manufacturing research conference 2014.
[31] Zhang Z, Ren H, Xu R, Moser N, Smith J, Ndip-Agbor E, et al. A mixed double-sided incremental forming toolpath strategy for improved geometric accuracy. J Manuf Sci Eng 2015;137(5):051007-1–1.
[32] Yoshikawa T, Nakamura K, Ueno K, Shima A. Study on incremental sheet metal bulging using tool bar (1). Proceedings of the 1999 Japanese spring conference on technology of plasticity 1999:305.
[33] Venkata Reddy N, Dixit PM. Department of Science and Technology, Government of India. Project no. SR/S3/MERC37/2007.
[34] Moser N, Pritchet D, Ren H, Ehmann KF, Cao J. An efficient and general finite element model for double-sided incremental forming. J Manuf Sci Eng 2016;138(9):091007-1–1.
[35] Moser N, Zhang Z, Ren H, Zhang H, Shi Y, Ndip-Agbor EE, et al. Effective forming strategy for double-sided incremental forming considering in-plane curvature and tool direction. CIRP Annals 2016;65(1):265–8.
[36] Lu B, Fang Y, Xu D, Chen J, Ai S, Long H, et al. Investigation of material deformation mechanism in double side incremental sheet forming. Int J Machine Tools Manuf 2015;93:37–48.
[37] Ren H, Moser N, Cao J. Simulation and analysis of double-sided incremental forming considering machine compliance. Proc 12th int conf on numerical methods in industrial forming process 2016:1–3.
[38] Leem D, Moser N, Ren H, Mozaffar M, Ehmann KF, Cao J. Improving the accuracy of double-sided incremental forming simulations by considering kinematic hardening and machine compliance. Procedia Manuf 2019;29:88–95.
[39] Bhattacharya A, Maneesh K, Venkata Reddy N, Cao J. Formability and surface finish studies in single point incremental forming. J Manuf Sci Eng 2011;133(6):061020-1–061021.
[40] Bansal A, Lingam R, Yadav SK, Reddy NV. Prediction of forming forces in single point incremental forming. J Manuf Process 2017;28:486–93.
[41] Timoshenko SP, Woinowsky-Krieger S. Theory of plates and shells. McGraw-hill New York; 1959.
[42] Silva M, Skjødt M, Martins PA, Bay N. Revisiting the fundamentals of single point incremental forming by means of membrane analysis. Int J Machine Tools Manuf 2008;48(1):73–83.
[43] Aerens R, Eyckens P, Van Bael A, Duflou J. Force prediction for single point incremental forming deduced from experimental and fem observations. Int J Adv Manuf Technol 2010;46(9–12):969–82.
[44] Ventsel E, Krauthammer T, Carrera E. Thin plates and shells: theory, analysis, and applications. Marcel Dekker. Inc New York; 2002.
[45] Wierzbicki T. Plates and shells. Lecture notes. Massachusetts Institute of Technology; 2006.
[46] Konka P, Lingam R, Upendra singh A, Shivaprasad CH, Reddy NV. Enhancement of accuracy in double sided incremental forming by compensating tool path for machine tool errors. Int J Adv Manuf Technol (accepted for publication)..